Neurobiology of Aging 89 (2020) 89–98

Contents lists available at ScienceDirect

Neurobiology of Aging

journal homepage: www.elsevier.com/locate/neuaging

Microglial activation arises after aggregation of phosphorylated-tau in a neuron-specific P301S tauopathy mouse model

Lynn van Olst [a,1,*], Daan Verhaege [a,b,c,1], Marc Franssen [a], Alwin Kamermans [a], Bart Roucourt [d], Sofie Carmans [d], Ellen Ytebrouck [d], Susanne M.A. van der Pol [a], Dennis Wever [a], Marko Popovic [a], Roosmarijn E. Vandenbroucke [b,c], Tomás Sobrino [e], Marijn Schouten [a], Helga E. de Vries [a,f]

[a] Department of Molecular Cell Biology and Immunology, Amsterdam Neuroscience, Amsterdam UMC, Amsterdam, the Netherlands
[b] VIB Center for Inflammation Research, Gent, Belgium
[c] Department of Biomedical Molecular Biology, Ghent University, Ghent, Belgium
[d] reMYND NV, Leuven, Belgium
[e] Clinical Neurosciences Research Laboratory, Department of Neurology, Clinical University Hospital, Health Research Institute of Santiago de Compostela, Spain
[f] Department of Medical Biochemistry, Amsterdam Cardiovascular Sciences, University of Amsterdam, Amsterdam, the Netherlands

ARTICLE INFO

Article history:
Received 8 March 2019
Received in revised form 2 January 2020
Accepted 6 January 2020
Available online 10 January 2020

Keywords:
Alzheimer's disease
FTD
Hyperphosphorylated tau
Microglia
P301S
Synapses

ABSTRACT

Alzheimer's disease, progressive supranuclear palsy and frontotemporal dementia are characterized by neuronal expression of aberrant tau protein, tau hyperphosphorylation (pTAU), tau aggregation and neurofibrillary tangle formation sequentially culminating into neuronal cell death, a process termed tauopathy. Our aim was to address at which tauopathy stage neuroinflammation starts and to study the related microglial phenotype. We used Thy1-hTau.P301S (PS) mice expressing human tau with a P301S mutation specifically in neurons. Significant levels of cortical pTAU were present from 2 months onwards. Dystrophic morphological complexity of cortical microglia arose after pTAU accumulation concomitant with increased microglial lysosomal volumes and a significant loss of homeostatic marker Tmem119. Interestingly, we detected increases in neuronal pTAU and postsynaptic structures in the lysosomes of PS microglia. Moreover, the overall cortical postsynaptic density was decreased in 6-month-old PS mice. Together, our results indicate that microglia adopt a pTAU-associated phenotype, and are morphologically and functionally distinct from wild-type microglia after neuronal pTAU accumulation has initiated.

1. Introduction

Intraneuronal aggregated tau inclusions, caused by tau hyperphosphorylation, are among the hallmarks of multiple neurodegenerative diseases such as Alzheimer's disease (AD), progressive supranuclear palsy, and other tauopathies including frontotemporal lobar degeneration (FTLD-tau) and related frontotemporal dementia (FTD) (Spillantini and Goedert, 2013). The development of tauopathies is a multistep process ultimately leading to neurofibrillary tangle (NFT) formation and neurodegeneration (Lee et al., 2001). Familial FTLD-tau/FTD associated with tau gene MAPT mutations demonstrate that tau aberrancies alone can be sufficient to cause neurodegeneration and dementia (Spillantini and Goedert, 2013). Similarly, mouse models expressing human tau harboring a P301S mutation, phenocopy a number of both behavioral and pathological properties observed in familial FTLD-tau/FTD cases (Allen et al., 2002; Takeuchi et al., 2011; Yoshiyama et al., 2007). Neuroinflammation is among these pathological properties frequently reported, yet the exact timing and consequences remain elusive (Streit et al., 2009; Yoshiyama et al., 2007). Microglia are the brain-resident immune cells that constantly scan their environment and initiate phagocytosis of pathogens and debris using their highly motile processes (Nimmerjahn et al., 2005; Sierra et al., 2013). Accordingly, on brain insults, microglia actively adapt their shape and function (Fernández-Arjona et al., 2017; Nimmerjahn et al., 2005; Sierra et al., 2013). The response of microglia toward

* Corresponding author at: Department of Molecular Cell Biology and Immunology, Amsterdam Neuroscience, Amsterdam UMC, De Boelelaan 1108, PO Box 7057, 1007 MB Amsterdam, the Netherlands. Tel.: +31204448080; fax: +31204448081.
E-mail address: l.vanolst@amsterdamumc.nl (L. van Olst).
[1] Authors contributed equally.

0197-4580/
https://doi.org/10.1016/j.neurobiolaging.2020.01.003

pathological tau is not completely understood, as spatiotemporal data regarding microglial morphology during the tauopathy process are currently lacking. Previous literature suggests that microgliosis may precede NFT formation and could thus be considered an early manifestation associated with the tau P301S mutation (Yoshiyama et al., 2007).

Furthermore, several groups have reported microglia to be in close contact with NFTs in AD brain tissue (Cras et al., 1991; Streit et al., 2009) and, owing to the phagocytic nature of microglia, they are thought to phagocytose neuronal content expressing pathological tau. This idea is partially supported by in vitro and ex vivo tau phagocytosis experiments (Brelstaff et al., 2018; Luo et al., 2015) and findings on human isolated tau species injected in the mouse brain (Bolós et al., 2017). However, in vivo experiments on phagocytosis of endogenously expressed neuronal pTAU in the brain are missing. Here, we describe that pTAU aggregation

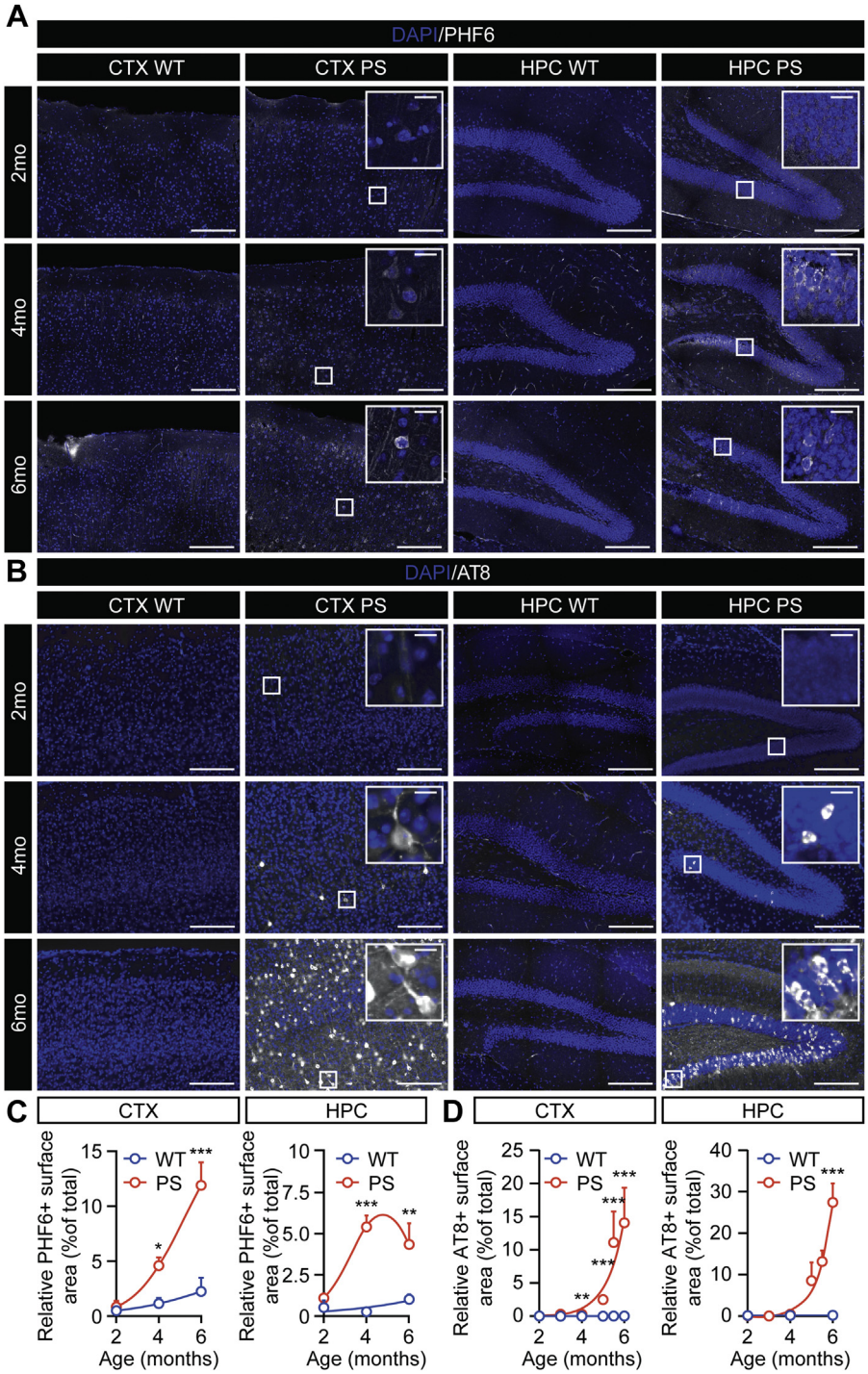

Fig. 1. Spatiotemporal PHF6 and AT8 expression immunohistochemistry analysis. (A) Micrographs displaying cortical and hippocampal PHF6 staining. (B) Micrographs displaying cortical and hippocampal AT8 staining. (C) Bar graphs displaying cortical and hippocampal pTAU PHF6+ surface area relative to total surface. (D) Bar graphs displaying cortical and hippocampal pTAU AT8+ surface area relative to total surface. Scale bars are 250 μm in overview images and 20 μm in the further magnified insets (A, B). Significant differences are indicated $^{*}p < 0.05$, $^{**}p < 0.01$, and $^{***}p < 0.001$, two-way ANOVA, $n = 3–4$ per experimental group (C, D).

precedes microglial activation in the cortex of Thy1-hTau.P301S (PS) mice. The pTAU-induced microglial phenotype observed consists of morphological dystrophy, loss of homeostatic markers, and lysosomal swelling. Interestingly, lysosomal swelling of PS microglia coincided with lysosomal localization of both pTAU and postsynaptic structures, together with an overall loss of cortical postsynaptic spine density.

2. Results and discussion

First, pTAU expression in PS and wild-type (WT) mice was assessed in a spatiotemporal manner using immunofluorescence of tau protein phosphorylation at Thr231 (PHF6) (Fig. 1A) and tau protein phosphorylation at Ser202 and Thr205 (AT8) (Fig. 1B, Figs. S1 and S2). Both PHF6 and AT8 identify pTAU forms early in tau inclusion formation, with PHF6 as one of the first belonging to the sequential cascade of phospho-epitopes to appear during pretangle formation in AD (Luna-Muñoz et al., 2007). In the cortex of PS mice, PHF6 and AT8 immunoreactivity increased significantly from 4 months onwards (Fig. 1), with PHF6 showing the earliest rise in signal. The pyramidal cell layer of the hippocampal cornus ammonum and granule cell layer of the hippocampal dentate gyrus of PS mice showed a significant albeit milder increase in PHF6+ and a slower increase in AT8+ signal from, respectively, 4- and 6-months forth (Fig. 1C–D), as reported previously (Allen et al., 2002). As the onset of cortical pTAU preceded that of the hippocampus, we next measured the degree of cortical pTAU aggregation using total (Fig. 2A–B), tris-soluble (Fig. 2C–D), and sarkosyl-insoluble (Fig. 2E–F) fractions by means of western blot analysis. These data indicated that levels of tris-soluble AT8 in the cortex

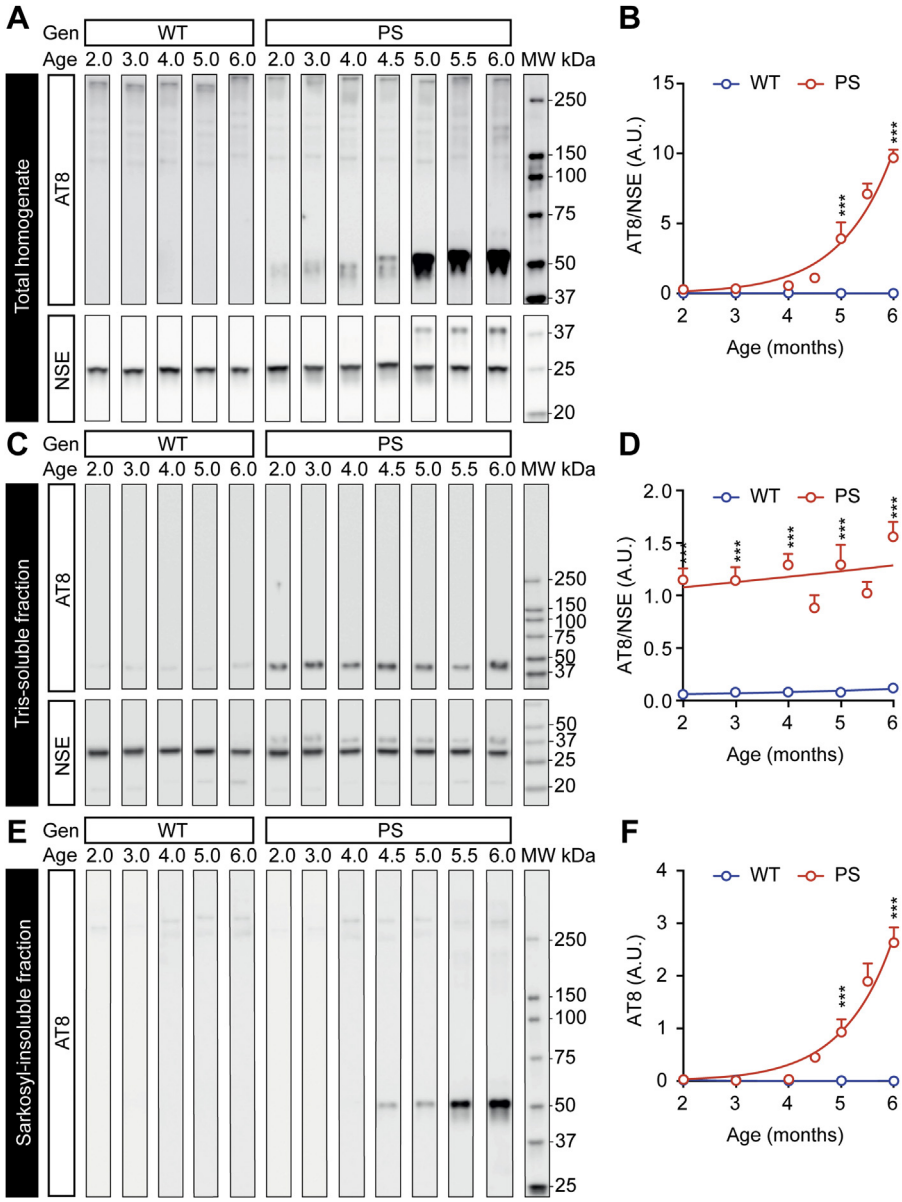

Fig. 2. Temporal soluble and insoluble cortical AT8 expression western blot analysis. (A) Representative blots displaying cortical total homogenate AT8 and neuron-specific enolase (NSE) loading control staining. (B) Bar graph displaying NSE normalized cortical total homogenate AT8 expression. (C) Representative blots displaying cortical Tris-soluble AT8 expression and NSE loading staining. (D) Bar graph displaying NSE normalized Tris-soluble cortical AT8 expression. (E) Representative blots displaying cortical sarkosyl-insoluble AT8 staining. (F) Bar graph displaying sarkosyl-insoluble cortical AT8 expression. Significant differences are indicated ***$p < 0.001$, WT versus PS mice, $n = 5$–10 per experimental group, two-way ANOVA.

were robustly present from 2 months onwards and subsequently started to aggregate from 5 months forth in PS mice.

Next, we measured the microglial response to pTAU aggregation by analyzing Iba1+ cell morphology in the cortex of PS mice using Sholl analysis (Fig. 3A). Different microglial morphophenotypes, although currently still under debate, appear to be associated with alterations in microglial activation status (Fernández-Arjona et al., 2019). As has been previously reported by us and others, aging

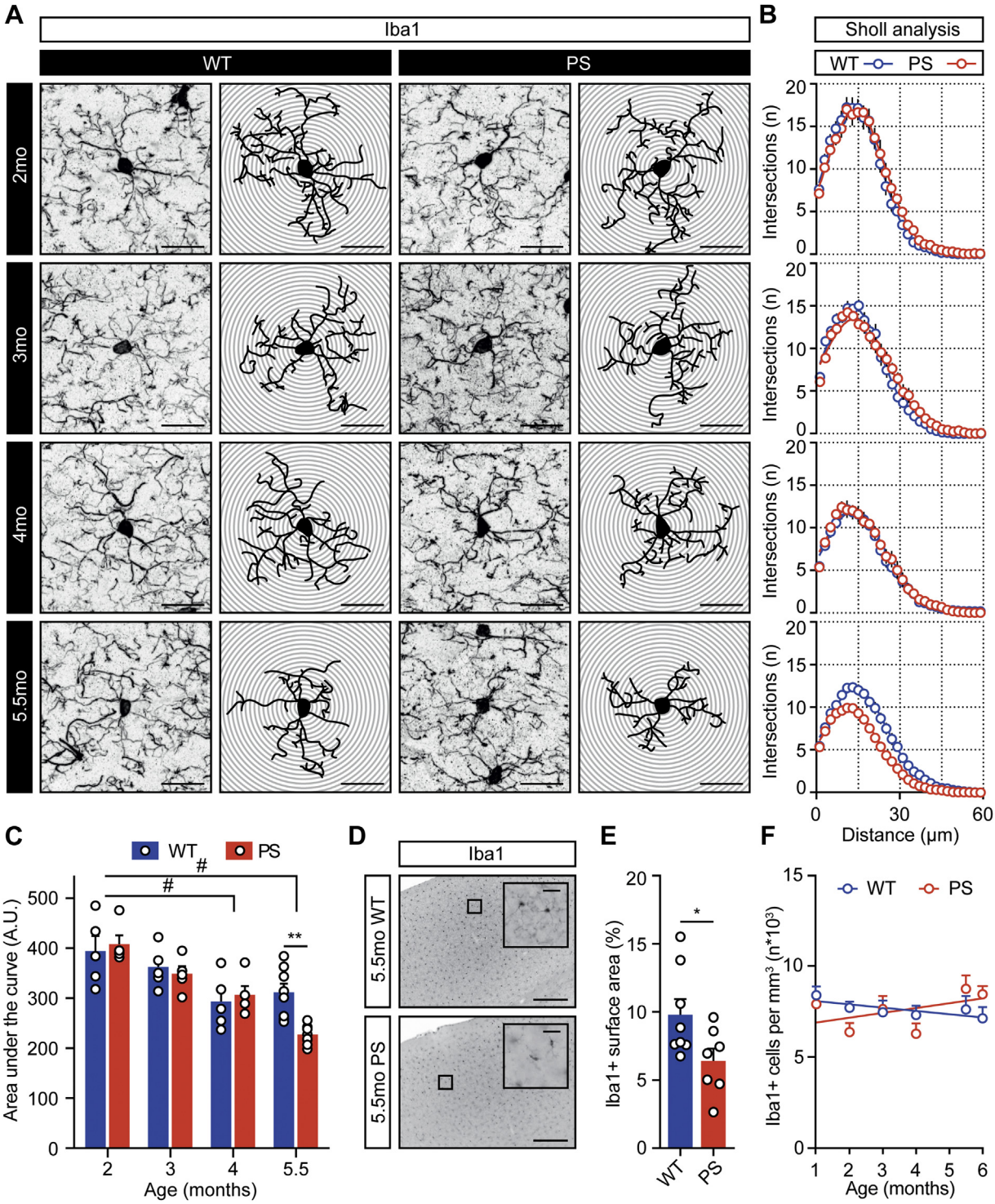

Fig. 3. Age- and genotype-associated changes in morphological complexity of cortical Iba1+ cells from PS mice. (A) Micrographs of cortical Iba1+ cells (top) and their respective traces (bottom). (B) Sholl plots per age displaying Iba1+ cell branch intersections per 2 μm steps from the cell soma. (C) Sholl-derived area under the curve (arbitrary units: A.U.) bar graph. (D) Micrographs of cortical Iba1+ cells. (E) Bar graph displaying the Iba1+ surface area at 5.5 months. (F) Plots displaying the number of Iba1+ cells per cortical mm^3. Scale bars = 20 μm (A), 500 μm overview (D) and 50 μm (D') in the further magnified insets. Significant differences are indicated, $^*p < 0.05$, $^{**}p < 0.01$ (genotype effect within age group), # $p < 0.05$ (age effect between age groups), two-way ANOVA (C, E). $N = 5–8$ per experimental group (B, C, E).

has a profound effect on microglia morphology (Streit et al., 2004; van Olst et al., 2018) and on genes expressed by microglia cells that are involved in cell adhesion, and actin (dis)assembly (Galatro et al., 2017). Indeed, we found a significant age-related reduction in Iba1+ cell complexity from 4 months onwards in the cortex of PS mice (Fig. 3A–C). A significant genotype effect, however, emerged later at 5.5 months of age with further decreases in cortical Iba1+ complexity (Fig. 3C). This reduced morphological complexity at 5.5 months of age coincided with a smaller area occupied by cortical Iba1+ cells in PS compared to WT mice (Fig. 3D–E) but not by a changed number of Iba1+ cells per area (Fig. 3F). These data indicate that a PS-induced microglia phenotype, as measured by microglia morphological complexity, arises approximately 3.5 months after the first detection of cortical PHF6 immunoreactivity (Fig. 1C) and soluble AT8 levels (Fig. 2C–D), and 2 weeks after the occurrence of insoluble AT8 aggregation (Fig. 2E–F). These findings might be compatible with those from Yoshiyama et al. reporting microglial activation to precede tangles in their prion-promoter–driven human tau P301S mouse model (Yoshiyama et al., 2007), as NFT formation follows tau hyperphosphorylation and aggregation. Our results combined with those reported by Yoshiyama et al. could imply that the timing of a microglial response to tau aberrancies occur in the final stages of early tau processing, yet before NFT formation (Yoshiyama et al., 2007). In the hippocampal regions of PS mice, we observed a milder and slower tau pathology (Fig. 1C–D) together with absence of a morphological response of microglia (Fig. S2). This mild kinetic is in accordance with observations of less severe tauopathy pathogenesis in the limbic system of human patients with FTD compared to other brain regions (Neary et al., 2005) and with the notion that microglia in the hippocampus are more immune vigilant (Grabert et al., 2016).

To understand whether the aforementioned cortical PS-induced microglial phenotype could be attributed to the recently described microglial neurodegenerative (MGnD) phenotype (Krasemann et al., 2017) or disease-associated microglial (DAM) phenotype (Keren-Shaul et al., 2017), we analyzed the expression of homeostatic microglia markers P2Y12 and Tmem119 in Iba1+ cells in the cortex at 5.5 months (Fig. 4). In accordance with a previous report (Litvinchuk et al., 2018), our results show that cortical microglia of PS mice display significantly decreased expression levels of Tmem119 (Fig. 4A–B) and a non-significant reduction in P2Y12 expression (Fig. 4C–D). These results suggest that pTAU-induced microglial activation might be accompanied by the MGnD/DAM phenotype.

We next analyzed microglial CD68 lysosome/endosome expression as a further measure for microglia activation. CD68+ volume within cortical Iba1+ cells (Fig. 5A) was mildly, yet significantly, higher in PS mice compared to WT mice at 5.5 months (Fig. 5B). The increase in Iba1+/CD68+ volume at 5.5 months (Fig. 5C) could not be explained by the unchanged number of CD68+ objects (Fig. 5D), but could be explained by the increased

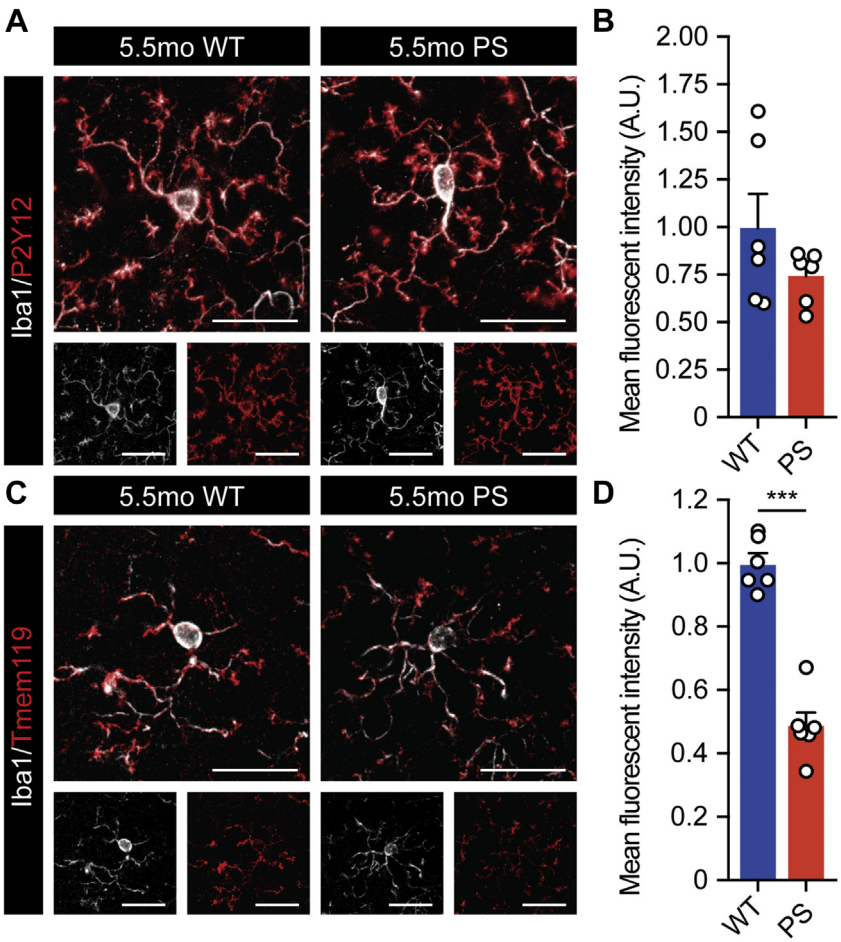

Fig. 4. Homeostatic microglia marker expression analysis of P2Y12 and Tmem119 in cortical Iba1+ cells from PS mice. (A) Maximum projection confocal micrograph displaying a representative cortical Iba1+/Tmem119+ microglia. (B) Bar graph displaying mean fluorescent intensity Tmem119 signal from Iba1+ microglia of 5.5-month-old WT and PS mice (arbitrary units: A.U.). (C) Maximum projection confocal micrograph displaying a representative cortical Iba1+/P2Y12+ microglia. (D) Bar graph displaying mean fluorescent intensity P2Y12 signal from Iba1+ microglia of 5.5-month-old WT and PS mice (arbitrary units: A.U.). Significant differences are indicated, ***$p < 0.001$, WT versus PS mice, $n = 6$ per experimental group, Student's t-test. Scale bars = 25 μm.

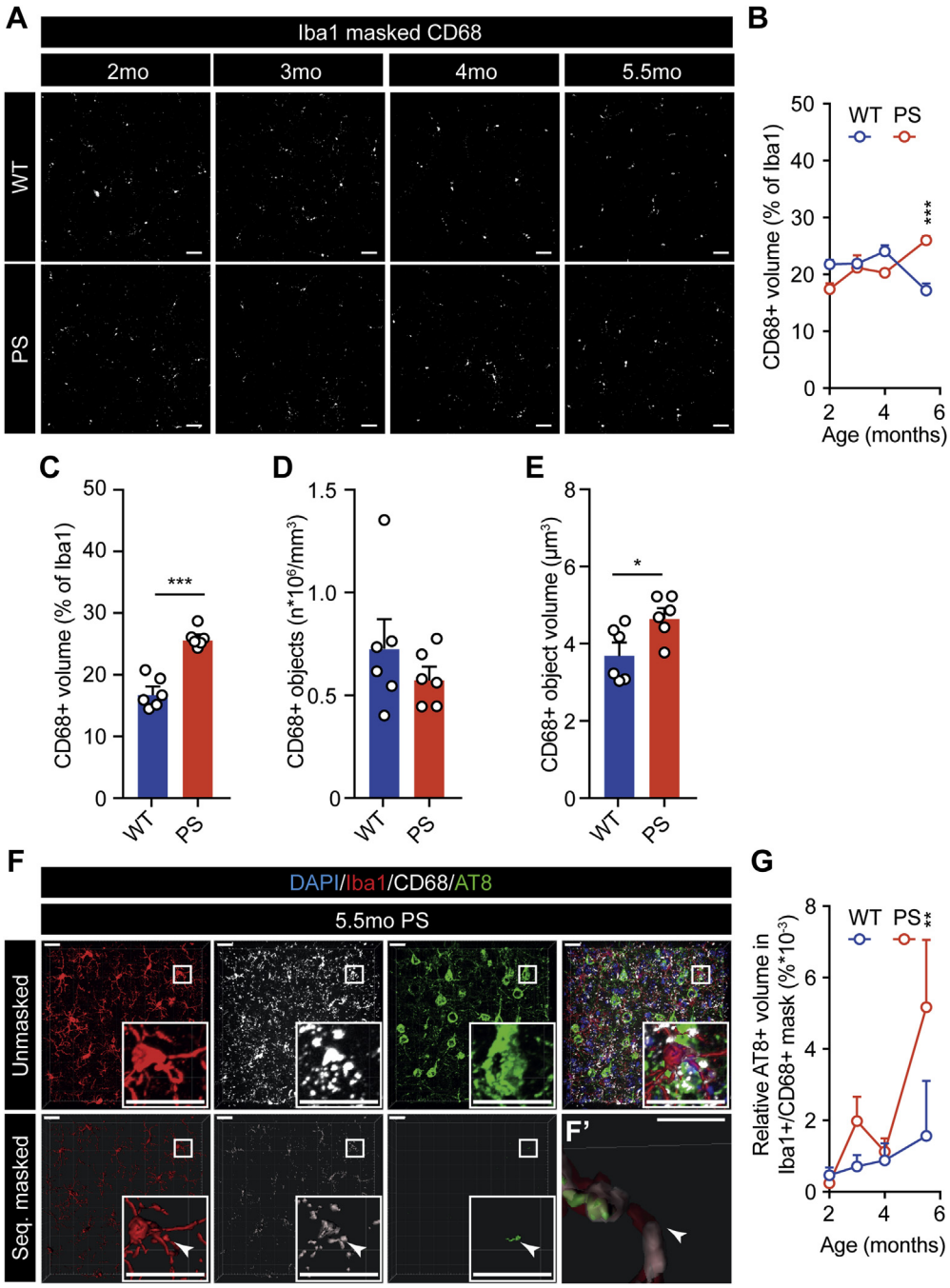

Fig. 5. Age- and genotype-associated changes in CD68+ object volume and AT8+ content of cortical Iba1+ cells from PS mice. (A) Micrographs displaying cortical CD68+ signal within cortical Iba1+ cells' mask. (B) Plots displaying the relative CD68+ volume in cortical Iba1+ cells. (C) Bar graph displaying the relative CD68+ volume in cortical Iba1+ cells at 5.5 months. (D) Bar graph displaying the number of CD68+ objects in cortical Iba1+ cells at 5.5 months. (E) Bar graph displaying the average volume of CD68+ objects in cortical Iba1+ cells at 5.5 months. (F) Representative unmasked micrographs displaying AT8+ cell engulfment by an Iba1+ cell (top) and AT8+ signal localized in sequentially masked Iba1+/CD68+ signal in the cortex of a 5.5-month-old PS mouse. Boxed areas are magnified in the bottom right corner of each image. Arrowheads indicate AT8+ signal within an Iba1+/CD68+ masked region of interest magnified in (F'). (G) Plots displaying the relative AT8+ volume within the Iba1+/CD68+ masked region of interest. Significant differences from two-way ANOVA (B and H) and Student's *t*-test (C, D, and E) are indicated $^{*}p < 0.05$, $^{**}p < 0.01$, $^{***}p < 0.001$, (genotype effect within age group). Scale bars = 20 µm (A and F) and 4 µm (F'). $N = 5–6$ per genotype.

average CD68+ object volume in cortical microglia of PS mice (Fig. 5E). These results suggest CD68+ lysosomes/endosomes to swell in cortical microglia of PS mice at 5.5 months.

We next hypothesized the lysosomal swelling to be related to microglial engulfment of both neuron-derived pTAU and synapses. Indeed, next to microglial engulfment of AT8+ neuronal structures, sequential masking of the Iba1+, CD68+, and AT8+ signal (Fig. 5F) revealed increases in lysosomal/endosomal pTAU content in cortical microglia of PS mice reaching significance at 5.5 months (Fig. 5G). These in vivo results suggest that microglial engulfment of pTAU leads to lysosome-mediated degradation, and complement preliminary engulfment data reported earlier from the same PS animals (Brelstaff et al., 2018). So far, several groups have reported on the phagocytic capacity of healthy microglia on challenge with extracellular sources of pTAU (Bolos et al., 2017; Luo et al., 2015). Whether this phagocytic capacity upholds when microglia are confronted

with an aged and neurodegenerated brain environment should be further investigated. Together, our data show that endogenously expressed neuron-derived pTAU results in microglial pTAU uptake. How microglia then process and/or are affected by pTAU uptake remains elusive. To our knowledge, we are the first to describe neuron-derived pTAU localization to microglial lysosomes of PS mice in vivo.

Interestingly, engulfed tau protein by microglia cells has been reported to enhance tau propagation throughout the brain via exosome secretion (Asai et al., 2015). Both microglia depletion (Asai et al., 2015) and blockade of microglia proliferation (Mancuso et al., 2019) in the early stages of the pTAU cascade were able to attenuate tau pathology and reduce neurodegeneration, whereas microglial depletion in aged tauopathy mice appeared not to affect tau burden (Bennett et al., 2018). In accordance with our results, this shows that in vivo, microglia are actively involved in phagocytosis and subsequent degradation of neuron-derived pathological tau species in the early stages of tau processing.

Furthermore, we analyzed postsynaptic density levels of Homer1+ spines in the cortex of PS mice at 6 months (Fig. 6A). We detected a decrease in Homer1+ postsynaptic spine density in the cortex of PS mice (Fig. 6B), which is in accordance with other studies that described synaptic loss in models of tauopathy (Hoffmann et al., 2013; Kopeikina et al., 2013). Recently, it was

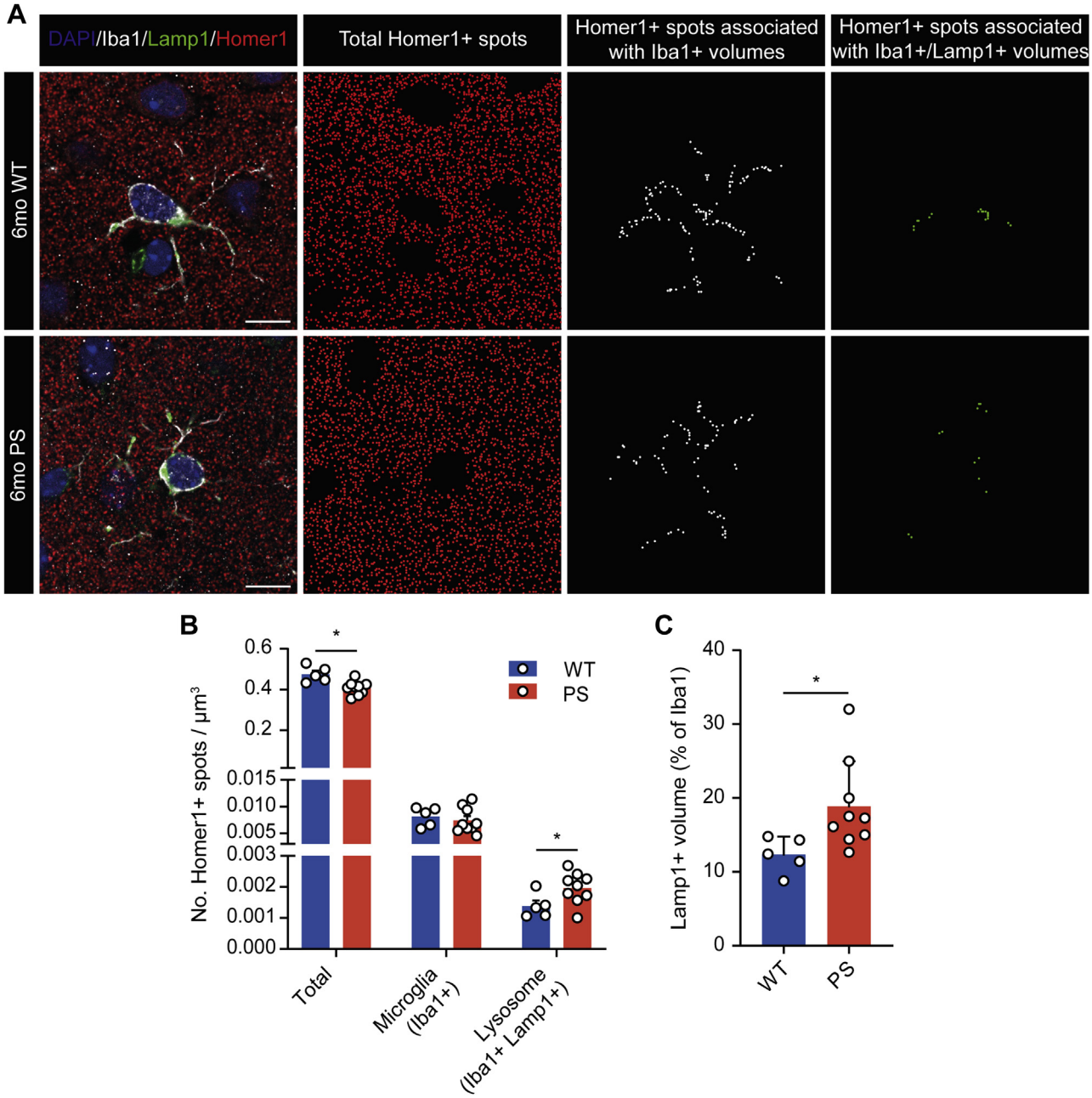

Fig. 6. Genotype-associated changes in Homer1+ spine density and spine engulfment by cortical Iba1+ cells from PS mice. (A) From left to right: Micrographs displaying cortical expression at 6 months of Iba1 (white), DAPI (blue), Lamp1 (green), and Homer1 (red); computed total Homer1+ spots; Homer1+ spots associated with Iba1+ volumes; Homer1+ spots associated with Iba1+ Lamp1+ volumes. (B) Bar graph displaying the number of Homer1+ spots (total; associated with Iba1+ volumes; associated with Iba1+/Lamp1+ volumes) per total volume (μm^3) at 6 months. (C) Bar graph displaying the relative Lamp1+ volume in cortical Iba1+ cells at 6 months. Scale bars = 10 µm (A). Significant differences from Student's *t*-tests (B, C) are indicated $^*p < 0.05$. $N = 5–9$ per genotype. (For interpretation of the references to color in this figure legend, the reader is referred to the Web version of this article.)

reported that microglia contribute to tauopathy-related spine loss by increased engulfment of synaptic spines (Dejanovic et al., 2018). While the number of total contacted Homer1+ spines by Iba1+ cells was unchanged (Fig. 6B), we did detect a significant increase in the number of Homer1+ postsynaptic structures in Lamp1+ lysosomes of Iba1+ cells in the cortex of PS mice (Fig. 6B). As such, part of the decline in cortical postsynaptic spine density may be mediated by microglia that actively participate in the phagocytosis of cortical synapses upon pTAU aggregation. In addition, we noted Lamp1+ lysosomal swelling in cortical microglia of PS mice at 6 months (Fig. 6C).

Microglial-mediated sculpting of neuronal circuits is critical for synaptic refinement and plasticity during development, but also plays a role in the pathogenesis of AD (Hong et al., 2016a,b; Rajendran and Paolicelli, 2018). Different mediators, such as those of the complement system, control this synaptic removal (Bialas and Stevens, 2013; Schafer et al., 2012; Stephan et al., 2012; Stevens et al., 2007). Interestingly, genes related to complement activation are differentially expressed in the CNS of young tauopathy mice and complement itself has been found to localize to neuronal pTAU (Ke et al., 2019). Together with our findings, these reports underline microglia to be actively involved in spine elimination and suggest that microglia actively reshape synapses in a tauopathy-induced neurodegenerative environment.

In conclusion, our results illustrate microglia to actively respond to neuronal pTAU aggregation in the early stages of tau processing. This microglial response included retraction of ramifications, swelling of lysosomes and the loss of homeostatic microglia markers such as P2Y12 and Tmem119. The increased lysosomal volumes of microglia were accompanied by lysosomal localization of both pTAU and postsynaptic structures. Interestingly, this pTAU-induced microglial phenotype coincided with an overall decrease in cortical postsynaptic density in PS mice. Altogether, our findings provide new insights suggesting microglia to actively respond to neuronal pTAU aggregation and give a timeframe for which tauopathy stage should be modulated to regulate microglial-mediated clearance of neuronal pTAU and cortical spines.

3. Materials and methods

3.1. Animals, tissue processing, and immunohistochemistry

Nontransgenic CBAxC57BL6 mice and homozygous Thy1-hTAU.P301S mice (Allen et al., 2002) in a CBAxC57BL6 background were maintained at the reMYND NV center (Leuven, Belgium). reMYND's accreditation number is LA1210532 and the number of the protocol approved by the Ethical Committee is 161103.R01. Mice were kept in cages with 12-hour light/dark cycles and food and water was available ad libitum. For the different experiments, groups of mice ($n \geq 5$ per group) were sacrificed at 2, 3, 4, 4.5, 5, 5.5, and 6 months of age. To do so, mice were anesthetized with ketamine, xylazin 2%, atropine, and saline (4:2.5:1:2.5). Temperature was monitored with a rectal thermometer and body temperature was maintained accordingly using a heating blanket. Once the body cavity was opened, the left ventricle was punctured for transcardial perfusion with a peristaltic pump and ice-cold saline for 3 minutes (3 mL/min). Simultaneously, the right atrium was cut to allow excess of liquid to escape. Next, the head was removed from the body and the brains were isolated from the skull. From here on, all tissues were randomized and samples were blinded. From every brain, the left hemisphere was postfixed with 4% paraformaldehyde in PBS and processed for western blotting as described in the respective section. The right hemisphere was postfixed overnight (4% PFA in PBS, 4 °C) and stored in PBS with 0.1% (v/w) sodium azide (4 °C) before sectioning. More specifically, per mouse, 40-μm thick sections at intervals of 160 μm were collected using a vibratome (VT1200, Leica) and stored in PBS at 4 °C for immunohistochemical analysis. For immunohistochemistry, the following primary (Table 1) and secondary (Table 2) antibodies were used. All sections were counterstained for DNA using DAPI (Invitrogen. 1:10,000).

3.2. Microscopy and morphological analysis

Immunostained brain sections were imaged using either a Zeiss imager D2 fluorescent microscope, a Nikon A1R confocal microscope or a Leica TCS SP8 HyD confocal microscope. For pTAU coverage, the thresholded AT8 and PHF6 signals were measured in the cortex and in the pyramidal cell layer of the hippocampal cornus ammonum and granule cell layer of the hippocampal dentate gyrus, using ImageJ and expressed as a relative surface area percentage of the total surface. Iba1+ cells were traced and analyzed using the Sholl Analysis Plugin (Ferreira et al., 2014) per animal as previously described (van Olst et al., 2018). All cells were traced manually by going through the z-stack/dimension and resulting 2D images were used as input to perform the aforementioned (standard Fiji-) Sholl analysis. Per animal, 6–14 cells were selected for tracing. Cells were randomly selected, but had to meet several inclusion criteria: 1) cells should be completely included within the z-stack borders of the image, 2) cells should not overlap with one another, and 3) cells should reside in the 2nd-3rd cortical layer. The area occupied by microglia was measured using Fiji software and determined from the Iba1+ area divided over the total surface area.

The expression of homeostatic markers Tmem119 and P2Y12 was measured within the thresholded Iba1+ mask to obtain fluorescence intensity solely from Iba1+ microglia. Fluorescence intensity was normalized to the intensity of Iba1.

For CD68 analysis, 2 sections per animal were analyzed. The Imaris ×64 software (version 9.1.2, Bitplane AG) was used to quantify microglial (Iba1+) and lysosomal/endosomal (CD68+) signals (e.g., number of objects, volume per identified object and total volume of all identified objects) in the individual corresponding channels. The lysosomal signal was masked by the microglial signal to obtain lysosomal information solely from lysosomes present inside Iba1+ microglia. The total volume of the microglial/lysosomal signal was then normalized by the volume of the imaged section (212.81 μm * 212.81 μm * 5 μm * number of z-stacks). Relative lysosomal volume (%) was calculated by dividing the total lysosomal volume by the total microglial volume per image. Per animal, all values were averaged from the individual images. Next, the identified lysosomes were used as a mask to search for AT8+ signals inside microglial lysosomes. The relative AT8 volumes (%) were calculated by dividing total AT8 volume by the

Table 1
Primary antibodies used

Antigen	Species	Dilution	Manufacturer	Cat. Number
CD68	Rat	1:400	Serotec	FA-11
Homer1	Rabbit	1:500	Synaptic Systems	160,003
Iba1	Rabbit	1:1000	Wako	019–19,741
Iba1	Goat	1:500	Abcam	ab5076
P2Y12	Rabbit	1:500	AnaSpec	55043A
pTAU (AT8)	Mouse	1:500	ThermoFisher	MN1020
pTAU (PHF6)	Mouse	1:400	Biolegend	828901
Tmem119	Rabbit	1:200	Abcam	ab209064

Key: CD68, cluster of differentiation 68; Homer1, homer protein homolog 1; Iba1, ionized calcium-binding adapter molecule 1; pTAU, Phospho-Tau; Tmem119, transmembrane protein 119.

Table 2
Secondary antibodies used

Antigen	Label	Species	Dilution	Manufacturer	Cat. Number
Mouse	Alexa488	Goat	1:500	Invitrogen	A28175
Rabbit	Alexa555	Goat	1:400	Invitrogen	A27039
Rat	Alexa647	Goat	1:500	Invitrogen	A21247
Goat	Alexa647	Donkey	1:400	Invitrogen	A21447

total lysosomal volume per image. Again, per animal, all values were averaged from 2 analyzed images.

For postsynaptic density analysis and synaptic engulfment by Iba1+ cells, 10–20 z-stacks were made per section per animal in the 3rd cortical layer. Each z-stack was focused to image a single Iba1+ cell with 2.5× zoom function using a 100× objective with a step size of 0.3 μm on a Leica TCS SP8 HyD confocal microscope. First, the Imaris x64 software (version 9.1.2, Bitplane AG) was used to make volumes of nuclei (DAPI), microglia (Iba1), lysosomes (Lamp1) and spots of postsynaptic terminals (Homer1) on 20 selected z-slices from the z-stack. To measure postsynaptic density, the Homer1+ spots were created with a spot diameter of 0.5 μm and a quality filter threshold of 1450. Unspecific Homer1+ reactivity in the cell nuclei was excluded by filtering out double positive DAPI+ Homer1+ spots. The final density of Homer1+ particles was calculated by dividing the number of spots by the total volume of the imaged section ((x * y * 0.3 μm * 20 z-slices)–DAPI volume). Per animal, all values were averaged from 10–20 analyzed images.

For engulfment of Homer1+ spines by Iba1+ cells, Kiss and Run XT analysis was performed in batch to create a new channel that displayed the distance between each Homer1+ spot and the Iba1+ and Lamp1+ volumes. Because Lamp1 is a general lysosomal marker that is not specific to microglia, created Lamp1 volumes that were negative for Iba1 expression were excluded. Iba1+ Homer1+ spots in direct contact with microglia processes and completely internalized Lamp1+ Iba1+ Homer1+ spots were selected and analyzed using the newly created distance-transformed channel by setting the distance-threshold between each spot and surface of interest to 0 μm. Finally, the interaction of microglia with Homer1+ synaptic terminals was calculated by dividing the number of contacted/internalized Iba1+ Homer1+ spots and the number of totally engulfed Lamp1+ Iba1+ Homer1+ spots by the total volume of the imaged section ((x * y * 0.3 μm * 20 z-slices) − DAPI volume). Relative lysosomal volume of Lamp1 (%) was calculated by dividing the total Lamp1+ volume by the total Iba1+ volume per image. Again, per animal, all values were averaged from 10–20 analyzed images.

3.3. Homogenization and differential extraction for western blot analyses

Differential extraction was performed after homogenizing the cortex with a potter-type mechanical homogenizer (VOS 14 S40, rate: 750 rpm; VWR) in 9 weight-volumes of ice-cold homogenization buffer, containing 20 mM Tris-HCl (pH 7.6), 150 mM NaCl, 1 mM ethylene diamine tetra acetic acid (EDTA, Merck), 1 mM ethylene glycol tetra acetic acid (EGTA, Sigma-Aldrich), 10 mM 1,10-ortho-phenanthroline monohydrate (Sigma-Aldrich), a cocktail of proteinase inhibitors (Complete, Roche, Germany), halt protease and phosphatase inhibitor (at a 2× concentration, Thermo Fisher Scientific, Belgium) and deacetylase inhibitors Trichostatin (1 μM, Sigma-Aldrich) and nicotinamide (5 mM, Sigma-Aldrich). A fixed volume of approximately half of the total homogenates (TotH) was centrifuged (136000 × g, 60 minutes, 4 °C; TLA-55 rotor, Optima TLX Ultracentrifuge, Beckman Coulter) to generate a Tris-soluble fraction (SF), whereas the remainder was stored at −80 °C. The supernatant (S1, further referred to as soluble fraction or SF) was separated from the pellet (P1), and stored at −80 °C. The pellet (P1) was solubilized in 9 weight-volumes high-salt (0.85 M NaCl) containing homogenization buffer. This fraction was centrifuged (20000 × g, 30 minutes, 4 °C) and the resulting high-salt pellet (P2) was stored at −80 °C. The supernatant (S2) was brought to 1% Sarkosyl with 10% Sarkosyl and incubated at room temperature for 60 minutes in a ThermoMixer (at room temperature) and then centrifuged (136000 × g, 60 minutes, 4 °C). The supernatant (S3, further referred to as Sarkosyl-soluble fraction or SSF) was stored at −80 °C. The pellet (P3) was resuspended in homogenization buffer (2 μL per mg tissue) and stored at −80 °C (further referred to as insoluble fraction or IF).

3.4. Polyacrylamide gel electrophoreses and western blotting

For application of conventional SDS-PAGE and western blotting, samples were denatured and reduced by incubation at 95 °C for 10 minutes after addition of SDS-PAGE sample buffer (XT sample buffer (4×) or Laemmli buffer, Bio-Rad; final concentration of 1× sample buffer with 2.5% (v/v) 2-mercaptoethanol). The samples were separated on either 7.5% Tris-HCl gels or 4%–12% Bis-Tris gels (Criterion XT Precast Gel, 26-well comb, 10 μL, 1.0 mm; Bio-Rad). After dry electro transfer (Trans-Blot Turbo Transfer System, Bio-Rad) to PVDF membranes (Trans-Blot Turbo Midi PVDF Transfer, Bio-Rad), the membranes were washed in Tris-buffered saline. Next, the membranes were incubated in Tris-buffered saline (pH 7.6) with 0.1% (v/v) Tween-20 containing 5% (w/v) nonfat dry milk for 1 hour at room temperature. Blots were incubated with the primary antibody overnight (1:500, AT8 Thermo Fisher Scientific, MN1020). After washing and incubation with an HRP-conjugated secondary antibody (goat-anti-mouse IgG, DAKO) blots were developed by the ECL detection system (LiteAblotR Plus ECL substrate, EuroClone; or SuperSignal West Femto Maximum Sensitivity Substrate, Thermo Fisher Scientific) and images were recorded digitally (VisionWorks Acquisition, UVP) with different exposure times. Dedicated software (VisionWorks Analysis, UVP) was used for analysis of the blots.

All TotH and SF blots were reprobed with anti-NSE (Abcam Ab16807; dilution 1:1000) as loading control. Samples were run in duplicate. For IF no suitable loading control is known. As multiple gels will be used for each antibody, reference samples of either TotH or SF fractions were run on each gel as an intergel reference. For the IF fractions, TotH reference material also was used on each gel.

3.5. Statistical analysis

All data reflect mean ± SEM and all comparisons were statistically tested in GraphPad Prism 8.2.1, using either unpaired two-tailed Student's *t*-tests for comparing 2 experimental groups, or two-way analysis of variance test when more than 2 groups were compared. With these statistical tests, significant differences are indicated and reflect the following *p*-values: $^{*}p < 0.05$, $^{**}p < 0.01$, and $^{***}p < 0.001$. Sholl analysis curves from which area under the curve data were deduced, were created, and analyzed using GraphPad Prism 8.2.1.

Disclosure statement

The authors declare no conflict of interest.

Acknowledgements

This work was financed by grants from Horizon 2020 #686009 to LO, MS, BR, TS, and HV and Miguel Servet Program CPII17/00027

to TS. The authors greatly appreciate both the AO|2M Microscopy Core Facility and Mike de Kok at the Amsterdam UMC location VUmc for their technical support.

Nontransgenic CBAxC57BL6 mice and homozygous Thy1-hTAU.P301S mice (Allen et al., 2002) in a CBAxC57BL6 background were maintained at the reMYND NV center (Leuven, Belgium). reMYND's accreditation number is LA1210532 and the number of the protocol approved by the Ethical Committee is 161103.R01.

Authors' contributions: LO, DV, MF, SC, EY, AK, SP, DW, and MS performed experiments and LO, DV, MF, BR, AK, MP, DW, and MS analyzed data. LO, DV, BR, AK, MS, and HV participated in experimental design, result discussion, interpretation and wrote the manuscript. LO, RV, TS, MS, and HV conceived and supervised the study.

Appendix A. Supplementary data

Supplementary data to this article can be found online at https://doi.org/10.1016/j.neurobiolaging.2020.01.003.

References

Allen, B., Ingram, E., Takao, M., Smith, M.J., Jakes, R., Virdee, K., Yoshida, H., Holzer, M., Craxton, M., Emson, P.C., Atzori, C., Migheli, A., Crowther, R.A., Ghetti, B., Spillantini, M.G., Goedert, M., 2002. Abundant tau filaments and nonapoptotic neurodegeneration in transgenic mice expressing human P301S tau protein. J. Neurosci. 22, 9340–9351.

Asai, H., Ikezu, S., Tsunoda, S., Medalla, M., Luebke, J., Haydar, T., Wolozin, Butovsky, O., Kügler, S., Ikezu, T., 2015. Depletion of microglia and inhibition of exosome synthesis halt tau propagation. Nat. Neurosci. 18, 1584–1593.

Bennett, R.E., Bryant, A., Hu, M., Robbins, A.B., Hopp, S.C., Hyman, B.T., 2018. Partial reduction of microglia does not affect tau pathology in aged mice. J. Neuroinflammation 15, 311.

Bialas, A.R., Stevens, B., 2013. TGF-β signaling regulates neuronal C1q expression and developmental synaptic refinement. Nat. Neurosci. 16, 1773–1782.

Bolós, M., Llorens-Martín, M., Perea, J.R., Jurado-Arjona, J., Rábano, A., Hernández, F., Avila, J., 2017. Absence of CX3CR1 impairs the internalization of Tau by microglia. Mol. Neurodegener 12, 59.

Brelstaff, J., Tolkovsky, A.M., Ghetti, B., Goedert, M., Spillantini, M.G., 2018. Living neurons with tau filaments aberrantly expose phosphatidylserine and are phagocytosed by microglia. Cell Rep. 24, 1939–1948.e4.

Cras, P., Kawai, M., Siedlak, S., Perry, G., 1991. Microglia are associated with the extracellular neurofibrillary tangles of Alzheimer disease. Brain Res. 558, 312–314.

Dejanovic, B., Huntley, M.A., De Mazière, A., Meilandt, W.J., Wu, T., Srinivasan, K., Jiang, Z., Gandham, V., Friedman, B.A., Ngu, H., Foreman, O., Carano, R.A.D., Chih, B., Klumperman, J., Bakalarski, C., Hanson, J.E., Sheng, M., 2018. Changes in the synaptic proteome in tauopathy and rescue of tau-induced synapse loss by C1q antibodies. Neuron 100, 1322–1336.e7.

Fernández-Arjona, M.D.M., Grondona, J.M., Granados-Durán, P., Fernández-Llebrez, P., López-Ávalos, M.D., 2017. Microglia morphological categorization in a rat model of neuroinflammation by hierarchical cluster and principal components analysis. Front Cell Neurosci. 11, 235.

Fernández-Arjona, M.D.M., Grondona, J.M., Fernández-Llebrez, P., López-Ávalos, M.D., 2019. Microglial morphometric parameters correlate with the expression level of IL-1β, and allow identifying different activated morphotypes. Front Cell Neurosci. 13, 472.

Ferreira, T., Blackman, A., Oyrer, J., Jayabal, A., Chung, A., Watt, A., Sjöström, J., van Meyel, D., 2014. Neuronal morphometry directly from bitmap images. Nat. Methods 11, 982–984.

Galatro, T.F., Holtman, I.R., Lerario, A.M., Vainchtein, I.D., Brouwer, N., Sola, P.R., Veras, M.M., Pereira, T.F., Leite, R.E., Möller, T., Wes, P.D., Sogayar, M.C., Laman, J.D., den Dunnen, W., Pasqualucci, C.A., Oba-Shinjo, S.M., Boddeke, E.W., Marie, S.K., Eggen, B.J., 2017. Transcriptomic analysis of purified human cortical microglia reveals age-associated changes. Nat. Neurosci. 20, 1162–1171.

Grabert, K., Michoel, T., Karavolos, M.H., Clohisey, S., Baillie, K.J., Stevens, M.P., Freeman, T.C., mmers, K., McColl, B.W., 2016. Microglial brain region–dependent diversity and selective regional sensitivities to aging. Nat. Neurosci. 19, 504–516.

Hoffmann, N.A., Dorostkar, M.M., Blumenstock, S., Goedert, M., Herms, J., 2013. Impaired plasticity of cortical dendritic spines in P301S tau transgenic mice. Acta Neuropathol. Commun. 1, 82.

Hong, S., Beja-Glasser, V.F., Nfonoyim, B.M., Frouin, A., Li, S., Ramakrishnan, S., Merry, K.M., Shi, Q., Rosenthal, A., Barres, B.A., Lemere, C.A., Selkoe, D.J., Stevens, B., 2016a. Complement and microglia mediate early synapse loss in Alzheimer mouse models. Science 352, 712–716.

Hong, S., Lasse Dissing, O., Stevens, B., 2016b. New insights on the role of microglia in synaptic pruning in health and disease. Curr. Opin. Neurobiol. 36, 128–134.

Ke, Y.D., Chan, G., Stefanoska, K., Au, C., Bi, M., Müller, J., Przybyla, M., Feiten, A., Prikas, E., Halliday, G.M., Piguet, O., Kiernan, M.C., Kassiou, M., Hodges, J.R., Loy, C.T., Mattick, J.S., Ittner, A., Kril, J.J., Sutherland, G.T., Ittner, L.M., 2019. CNS cell type-specific gene profiling of P301S tau transgenic mice identifies genes dysregulated by progressive tau accumulation. J. Biol. Chem. 294, 14149–14162.

Keren-Shaul, H., Spinrad, A., Weiner, A., Matcovitch-Natan, O., Dvir-Szternfeld, R., Ulland, T.K., David, E.1, Baruch, K., Lara-Astaiso, D., Toth, B., Itzkovitz, S., Colonna, M., Schwartz, M., Amit, I., 2017. A unique microglia type associated with restricting development of Alzheimer's disease. Cell 169, 1276–1290.e17.

Kopeikina, K.J., Polydoro, M., Tai, H.C., Yaeger, E., Carlson, G.A., Pitstick, R., Hyman, B.T., Spires-Jones, T.L., 2013. Synaptic alterations in the rTg4510 mouse model of tauopathy. J. Comp. Neurol. 521, 1334–1353.

Krasemann, S., Madore, C., Cialic, R., Baufeld, C., Calcagno, N., El Fatimy, R., Beckers, L., O'Loughlin, E., Xu, Y., Fanek, Z., Greco, D.J., Smith, S.T., Tweet, G., Humulock, Z., Zrzavy, T., Conde-Sanroman, P., Gacias, M., Weng, Z., Chen, H., Tjon, E., Mazaheri, F., Hartmann, K., Madi, A., Ulrich, J.D., Glatzel, M., Worthmann, A., Heeren, J., Budnik, B., Lemere, C., Ikezu, T., Heppner, F.L., Litvak, V., Holtzman, D.M., Lassmann, H., Weiner, H.L., Ochando, J., Haass, C., Butovsky, O., 2017. The TREM2-APOE pathway drives the transcriptional phenotype of dysfunctional microglia in neurodegenerative diseases. Immunity 47, 566–581.e9.

Lee, V.M., Goedert, M., Trojanowski, J.Q., 2001. Neurodegenerative tauopathies. Annu. Rev. Neurosci. 24, 1121–1159.

Litvinchuk, A., Wan, Y.W., Swartzlander, D.B., Chen, F., Cole, A., Propson, N.E., Wang, Q., Zhang, B., Liu, Z., Zheng, H., 2018. Complement C3aR inactivation attenuates tau pathology and reverses an immune network deregulated in tauopathy models and Alzheimer's disease. Neuron 100, 1337–1353.e5.

Luna-Muñoz, J., Chávez-Macías, L., García-Sierra, F., Mena, R., 2007. Earliest stages of tau conformational changes are related to the appearance of a sequence of specific phospho-dependent tau epitopes in Alzheimer's Disease1. J. Alzheimers Dis. 12, 365–375.

Luo, W., Liu, W., Hu, X., Hanna, M., Caravaca, A., Paul, S.M., 2015. Microglial internalization and degradation of pathological tau is enhanced by an anti-tau monoclonal antibody. Sci. Rep. 5, 11161.

Mancuso, R., Fryatt, G., Cleal, M., Obst, J., Pipi, E., Monzón-Sandoval, J., Ribe, E., Winchester, L., Webber, C., Nevado, A., Jacobs, T., Austin, N., Theunis, C., Grauwen, K., Daniela Ruiz, E., Mudher, A., Vicente-Rodriguez, M., Parker, C.A., Simmons, C., Cash, D., Richardson, J., , NIMA Consortium, Jones, D.N.C., Lovestone, S., Gómez-Nicola, D., Perry, V.H., 2019. CSF1R inhibitor JNJ-40346527 attenuates microglial proliferation and neurodegeneration in P301S mice. Brain 42, 3243–3264.

Neary, D., Snowden, J., Mann, D., 2005. Frontotemporal dementia. Lancet Neurol. 4, 771–780.

Nimmerjahn, A., Kirchhoff, F., Helmchen, F., 2005. Resting microglial cells are highly dynamic surveillants of brain parenchyma in vivo. Science 308, 1314–1318.

Rajendran, L., Paolicelli, R.C., 2018. Microglia-mediated synapse loss in Alzheimer's disease. J. Neurosci. 38, 2911–2919.

Schafer, D.P., Lehrman, E.K., Kautzman, A.G., Koyama, R., Mardinly, A.R., Yamasaki, R., Ransohoff, R.M., Greenberg, M.E., Barres, B.A., Stevens, B., 2012. Microglia sculpt postnatal neural circuits in an activity and complement-dependent manner. Neuron 74, 691–705.

Sierra, A., Abiega, O., Shahraz, A., Neumann, H., 2013. Janus-faced microglia: beneficial and detrimental consequences of microglial phagocytosis. Front Cell Neurosci. 7, 6.

Spillantini, M.G., Goedert, M., 2013. Tau pathology and neurodegeneration. Lancet Neurol. 12, 609–622.

Stephan, A.H., Barres, B.A., Stevens, B., 2012. The complement system: an unexpected role in synaptic pruning during development and disease. Annu. Rev. Neurosci. 35, 369–389.

Stevens, B., Allen, N.J., Vazquez, L.E., Howell, G.R., Christopherson, K.S., Nouri, N., Micheva, K.D., Mehalow, A.K., Huberman, A.D., Stafford, B., Sher, A., Litke, A.M., Lambris, J.D., Smith, S.J., John, S.W., Barres, B.A., 2007. The classical complement cascade mediates CNS synapse elimination. Cell 131, 1164–1178.

Streit, W.J., Sammons, N.W., Kuhns, A.J., Sparks, D.L., 2004. Dystrophic microglia in the aging human brain. Glia 45, 208–212.

Streit, W.J., Braak, H., Xue, Q.S., Bechmann, I., 2009. Dystrophic (senescent) rather than activated microglial cells are associated with tau pathology and likely precede neurodegeneration in Alzheimer's disease. Acta Neuropathol. 118, 475–485.

Takeuchi, H., Iba, M., Inoue, H., Higuchi, M., Takao, K., Tsukita, K., Karatsu, Y., Iwamoto, Y., Miyakawa, T., Suhara, T., Trojanowski, J.Q., Lee, V.M., Takahashi, R., 2011. P301S mutant human tau transgenic mice manifest early symptoms of human tauopathies with dementia and altered sensorimotor gating. PLoS One 6, e21050.

van Olst, L., Bielefeld, P., Fitzsimons, C.P., de Vries, H.E., Schouten, M., 2018. Glucocorticoid-mediated modulation of morphological changes associated with aging in microglia. Aging Cell 17, e12790.

Yoshiyama, Y., Higuchi, M., Zhang, B., Huang, S.M., Iwata, N., Saido, T.C., Maeda, J., Suhara, T., Trojanowski, J.Q., Lee, V.M., 2007. Synapse loss and microglial activation precede tangles in a P301S tauopathy mouse model. Neuron 53, 337–351.